Heliyon 6 (2020) e04533

Contents lists available at ScienceDirect

Heliyon

journal homepage: www.cell.com/heliyon

Research article

A novel synthesis of graphene quantum dots via thermal treatment of crude graphite oxide in a dry and alkaline condition, and their application in uranyl detection

Shanli Yang [a,1], Yingru Li [a,*,1], Shaofei Wang [a], Jingsong Xu [b], Lang Shao [a], Tao Gai [a], Hao Tang [a], Yiming Ren [a], Mingfu Chu [a,**], Bianyuan Xia [a]

[a] Institute of Materials, Chinse Academy of Engineering Physics, Mianyang, Sichuan province, 621700, China
[b] Science and Technology on Surface Physics and Chemistry Laboratory, P.O. Box Nos, 9-35, Huafengxincun, Jiangyou City, Sichuan Province, 621908, China

ARTICLE INFO

Keywords:
Analytical chemistry
Environmental science
Materials science
Graphene dots
Uranyl
Detection
Fluorescence quenching

ABSTRACT

In this article, a novel method to synthesize graphene quantum dots was developed via thermal treatment of crude graphite oxide (GO) in a dry and alkaline condition to cut the crude GO sheets into small graphene quantum dots (named as aGQDs). The aGQDs are nano-scale reduced graphene oxide pieces with the sizes around 5–10 nm. The aGQDs could disperse in water for their richment of oxygen-containing groups. The fluorescence properties were carefully investigated. The aGQDS aqueous solution shows a bright yellow-green fluorescence under the UV illumination. Besides, the uranyl ions show a strong fluorescence quenching effect on the a aGQD aqueous solution even at a low concentration ($\sim 10^{-7}$ M) compared with other common ions in natural water-body, which makes that these aGQDs could be applied as a chemosensor for detection of uranyl ions with good sensitivity and selectivity.

1. Introduction

Uranium is the key fuel material applied in nuclear industry, which at the same time is also a radioactive and toxic element showing significantly adverse impact on human health as well as all living creatures [1, 2, 3, 4]. Nowadays, owing to the global energy issues, nuclear industry is experiencing a rapid development. Expectedly, the public attention on nuclear leakage accidents is also arising in the meanwhile, especially after Fukushima nuclear accident [5, 6]. Uranium could appear in various valence states, while hexavalent form (UO_2^{2+}) is the most stable state in natural environment, which possesses high aqueous solubility, easy mobility and the maximum bioavailability [7, 8, 9]. Due to the environmental and public-health concern, the detection of trace level of uranyl contamination in natural circumstance is of crucial importance and draws increasing attraction. Several instrumental techniques have been employed, such as atomic absorption spectrometry (AAS) [10], inductively coupled plasma mass spectroscopy (ICP-MS) [11], total reflection X-ray fluorescence spectrometry (TR-XRF) [12], cold-vapor atomic fluorescence spectrometry [13], laser-induced kinetic phosphorimetry [14], surface enhanced Raman spectroscopy [15], etc. Although possessing high accuracy and ultra-low detection limit, these techniques involve expensive instruments, together with complex and time-consuming sample preparation procedure, making them improper for online, rapid and qualitative analysis abroad in natural environment [16, 17, 18]. Thus, it is still an urgent issue to develop facile and convenient methods to detect uranyl in aqueous environments and fluorescent chemosensor is identified as one of the most attractive and potential tools for fast and handy determination of uranyl ions.

Carbon quantum dots (CQDs) have become fascinating nano carbon materials during last decades, because of their fluorescence property, stability, low toxicity, etc. [19, 20, 21, 22], showing great potentials in a variety of applications, such as bioimaging [23], catalysts [24, 25, 26] and optoelectronics [27, 28, 29, 30]. Especially, due to the CQDs' rich oxygen-containing groups or other functional groups decorated via modification, they show strong interaction with certain metal cations even at ultra-low concentrations, followed by significant and visible fluorescence quenching effect [18, 31, 32, 33, 34]. In other words, it is a promising fluorescent chemosensor material for facile and rapid uranyl

* Corresponding author.
** Corresponding author.
E-mail addresses: liyingru@caep.cn (Y. Li), chumingfu@caep.cn (M. Chu).
[1] Shanli Yang and Yingru Li contributed to this article equally.

https://doi.org/10.1016/j.heliyon.2020.e04533
Received 19 June 2019; Received in revised form 19 January 2020; Accepted 20 July 2020

detection [35, 36]. Generally, synthesis routes of CQDs could be classified into two main kinds: top-down and bottom-up process. Top-down methods refer to cutting small pieces from certain carbon sources to form CQDs; while bottom-up methods usually start from small molecule precursors to form high-molecular-weight CQDs via polymerizing and carbonization [37]. The top-down methods reported before employed different kinds of techniques, including high resolution electron-beam [19], chemical [38] or electrochemical [39] oxidation, hydrothermal treatment [40] or microwave assisted reactions [41]. These methods usually suffer from the extreme experimental conditions such as high voltage, strong acidic medium, strong oxidizing conditions or long reaction time, which inhibit the further application and involve large-scale production [42].

In this article, a novel and relative mild method is developed for the fast synthesis of small graphene quantum dot (aGQD) via thermal treatment of crude graphite oxide (GO) sheets in a dry and alkaline condition. The aGQDs show bright yellow-green luminescence and exhibit stable fluorescence properties in a wide pH range. Moreover, the uranyl ion exhibits a strong fluorescence quench effect on the aGQD aqueous solution even at a low concentration ($\sim 10^{-7}$ M), while other common interference ions show a much weaker fluorescence quench effect, showing that a fluorescent chemosensor with good sensitivity and selectivity is successfully constructed for uranyl ion detection based on these aGQDs.

2. Experimental section

2.1. Materials

Analytical grade chemicals were used throughout the investigation. Graphite powders (300 mesh) were purchased from Alfa Aesar (USA). $KMnO_4$, H_2SO_4, H_2O_2, HCl, KOH, and NaOH were bought from Sinopharm Chemical Reagent Co. Ltd. $UO_2(NO_3)_2$ was bought from Dingtian Chemical Co. Ltd. (Xi'an, China). The uranyl nitrate solution was prepared via dissolving uranyl nitrate in de-ionic water. The uranium concentration of the parent solution was controlled around 10^{-3} M, and the testing solutions were prepared by diluting it. The pH of the uranyl nitrate solution was adjusted by NaOH and HCl.

2.2. Synthesis of crude GO powders

Crude GO powders were prepared by oxidation of natural graphite powder using a modified Hummers' method according to our previously report [43, 44, 45]. The crude GO powders were smashed into small and homogenous powders, and sieved via a 1200 mesh sieve before further treatments.

2.3. Synthesis of aGQD

Firstly, KOH (20 g) was dissolved in ethanol/water solvent (25 mL, $v_{ethanol}/v_{water} = 4{:}1$) to form a strong alkaline solution. Crude GO powders (5 g) were added into the solution slowly under agitation, to avoid severely boiling. A kind of black and viscid paste was obtained. Then the black paste was dried at 80 °C, and successively the resulting black solid was put into a muffle furnace and then it was heated to 300 °C ambient at a rate of 10 °C min^{-1} and kept at this temperature for 4 h in the ambient atmosphere. Successively, the sample was washed by deionized water, and the aGQDs came into the filtrate with other water-soluble impurities. The filtrate was purified by dialysis for two weeks using a dialysis membrane with a molecular weight cutoff of 1000 g mol^{-1} to remove the remaining impurities. Then the GQDs aqueous dispersion was obtained. Finally, the aGQDs aqueous dispersion was further concentrated to achieve desirable concentration by rotary evaporator. The concentration was measured by weighting the solid after freezing drying 5 mL of the dispersion.

2.4. Characterization

Transmission electronic microscope (TEM) images were collected on a JEM-2010 microscope (JEM-2010, Japan). UV-visible spectra were obtained on a U-3010 UV-visible spectrometer (Hitachi, Japan). The samples were also analyzed with a Raman microscope with 512 nm laser excitation (Horba JobinYvon, France) and Fourier transform infrared spectroscopy (Spectrum GX FT-IR spectrometer, PerkinElmer). Fluorescence spectra were measured by using a Luminar fluorescence spectrometer (PerkinElmer), and the concentrations of the aqueous dispersions of aGQDs were controlled to be around 0.05 mg mL^{-1}.

2.5. Detection of uranyl ions

Typically, 2 mL 0.05 mg mL^{-1} aGQDs dispersion was put into cuvette after optimizing pH. Then 20 μL 10^{-5} uranyl solution was added into the aGQDs solution gradually. Then till the fluorescence spectra were stable, they were recorded. To evaluate the selectivity of aGQDs as chemosensors, different interference ions were added into aGQDs solution respectively and the final concentration was controlled at 10^{-5} M.

3. Results and discussion

3.1. Synthesis process and mechanism

The process of synthesizing aGQDs is illustrated in Figure 1. Step 1 is a typical Hummers' oxidization of graphite powders, which effectively exfoliates graphite and introduces large quantities oxygen-containing groups into the graphene sheets. In Step 2, the crude GO powders are mixed with KOH. Under strong alkaline condition, deoxygenation of GO by the disproportionation reaction would occur, resulting in formation of CO_2, vacancy defects and extension of conjugation based on the Dynamic Structural Model (DSM) developed by Tour *et al* [46]. Thus, two probable phenomena would take place as the vacancy defects enlarge: 1) small fragments might generate from the main bodies of GO sheets; 2) some fragments' chemical bonding connections with the main bodies of GO sheets, though do not disappear, are weakened. This is the main physical chemistry basis for the preparation of aGQD. Step 3 is a thermal treatment at 300 °C under the ambient air atmosphere. The oxidization of oxygen makes that more fragments with weak chemical bonding connections the main bodies of GO sheets are cut down and transferred into aGQDs. At the same time, due to the decarboxyl reaction of the GO at high temperature, the hydrophilic GO sheets are reduced into hydrophobic RGO sheets, making that the aqueous soluble aGQDs are facile to separate from the RGO sheets by simple washing in Step 4. It should be emphasized here that, when the temperature reaches 500 °C or even higher, no aGQDs could be obtained due to the strong oxidization of oxygen. After dialysis to remove the residual impurities, the aGQDs are obtained. This is a time-saving process compared with the other methods via cutting GO or rGO; for the processes of preparing and purifying a GO precursor from graphite usually needs more than 10 days. Moreover, in comparison with combustion of potassium–graphite, microwave-hydrothermal treatment in acid, high voltage electron-beam, oxidization in sulfuric acid, this method can be carried out under a relatively mild circumstance.

3.2. Morphology and structure

Like other kinds of CQDs reported before [37], the sizes of aGQDs are mainly in a narrow range around 5–14 nm (Figure 2a, c). The sizes are mostly distributed from 8 nm to 13 nm, and a small portion of aGQDs have the sizes less than 6 nm. The HRTEM image gives the detailed information of the aGQDs' microscopic structure (Figure 2b). As can be seen, aGQDs possess a random layer lattice rather than a clear lattice fine structure, implying that the conjugated regions are partially destructed

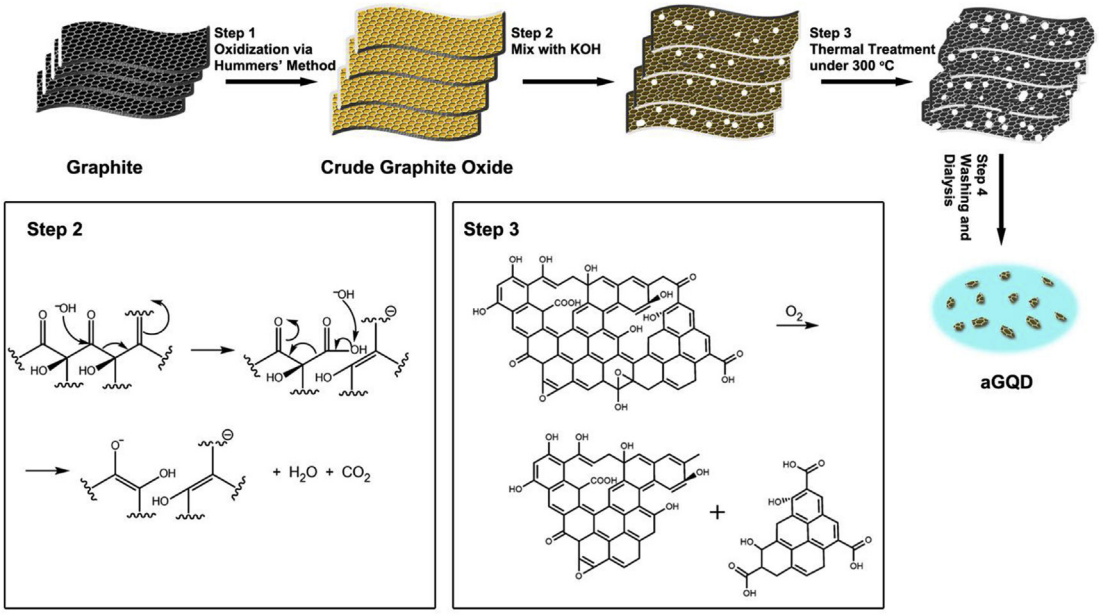

Figure 1. Illustration of synthesis procedures of the aGQDs and the possible reaction mechanism in step 2 and step 3.

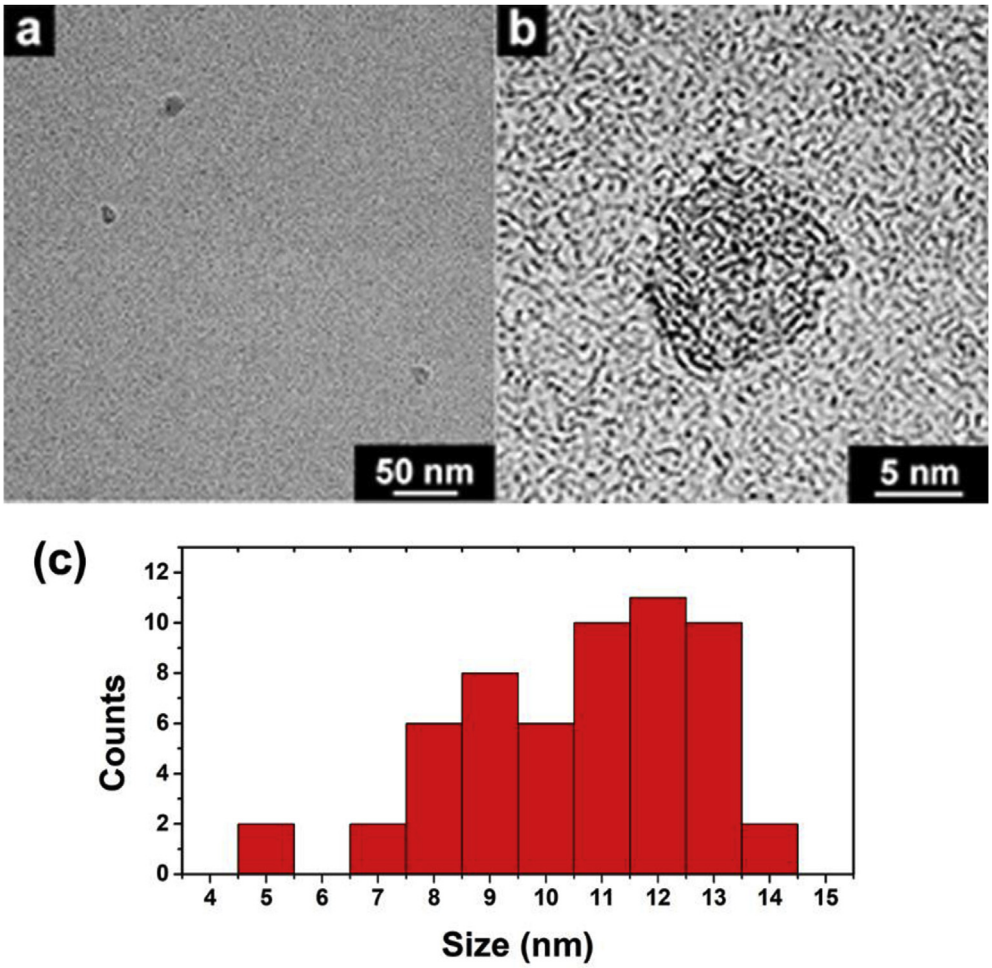

Figure 2. (a), (b) TEM images of aGQDs with different magnifications; (c) Size distribution of aGQDs counted from 15 TEM images.

by the strong oxidization in the procedures of preparing GO via Hummers' method and the successive thermal treatment.

The chemical structure of aGQDs were investigated by UV-Vis adsorption, Fourier-transform Infrared (FT-IR) and Raman spectra. The UV-Vis spectrum of 0.05 mg mL^{-1} aGQD solution is shown in Figure 3a. A shoulder absorption peak at 260 nm is observed which is ascribed to the π–π* transition of aromatic sp^2 domains, similar to chemically reduced GO [35, 45]. Another weak shoulder peak in the region of about 300 nm should be related to the n–π* transition [38]. The FT-IR spectra provides characteristic information of aGQDs' functional groups (Figure 3b). The significant characteristic peaks at about 3300 cm^{-1} and 1701 cm^{-1} are associated with the vibrations of O–H and C=O groups, respectively. The emerging peaks at 2300 cm^{-1}, 1600 cm^{-1} should be related with the presence of O=C=O, aromatic carbons, respectively. The peaks at 1381 cm^{-1} and 1255 cm^{-1} shows the presence of epoxy groups [37, 42, 47].

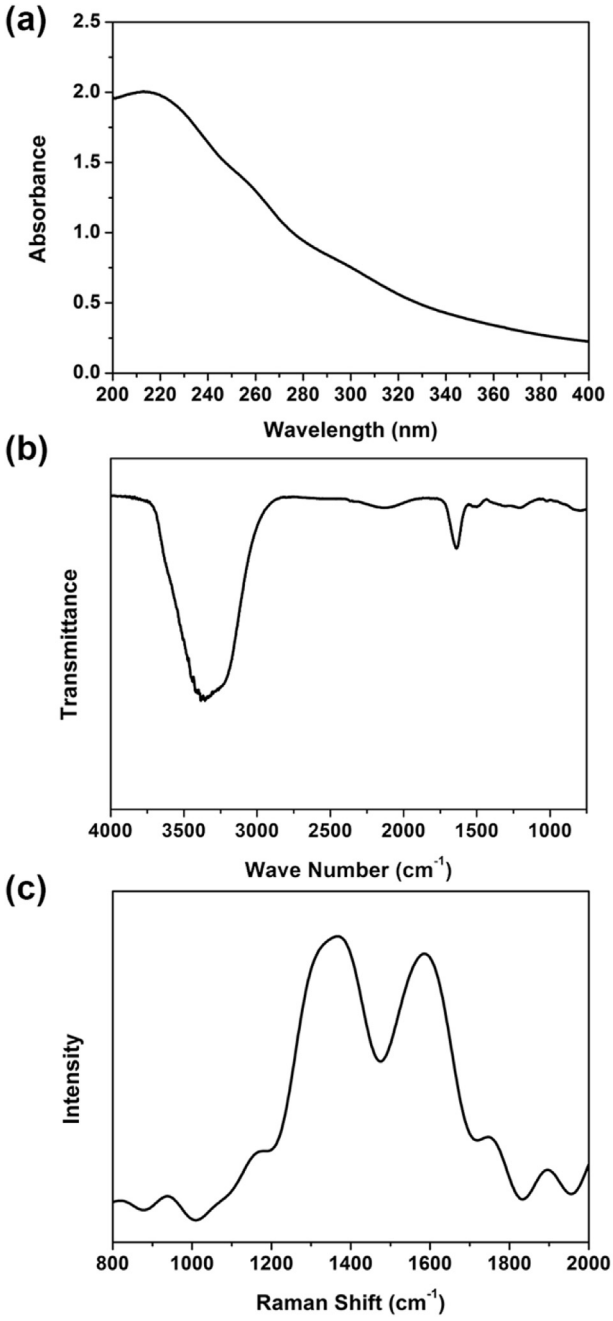

Figure 3. a) UV-Vis spectrum of 0. 05 mg mL^{-1} aGQDs solution; b) FT-IR spectrum of 0.05 mg mL^{-1} aGQDs solution; c) Raman spectrum of freezing dried aGQDs powders.

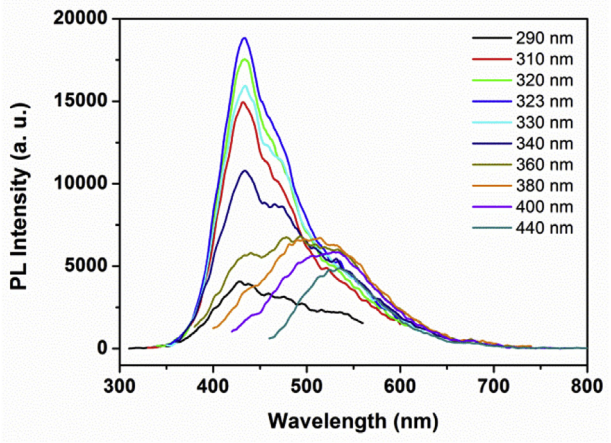

Figure 4. PL spectra of 0.05 mg mL^{-1} at different excitation wavelengths (pH = 5).

These results exhibit that even though these aGQDs experience thermal treatment, they still possess a large quantity of oxygen-containing functional groups such as carboxylic acid, epoxy, alkoxy, hydroxyl and carbonyl groups on their edges or surfaces, making them soluble in aqueous solution. What is more, the rich oxygen-containing groups would show strong coordination effect with the uranyl ions, which is the basic chemical principle of the quenching effect. The Raman spectrum of freezing dried aGQDs has two bands at 1365 cm^{-1} and at 1605 cm^{-1} respectively, named as D-band and G-band. G-band is associated with the regular graphitic domains, while D-band is associated with the defects. The intensity ratio I_D/I_G is calculated to be 1.08 (Figure 3c), similar to those of other rGO materials [44, 45]. To sum up, the results above

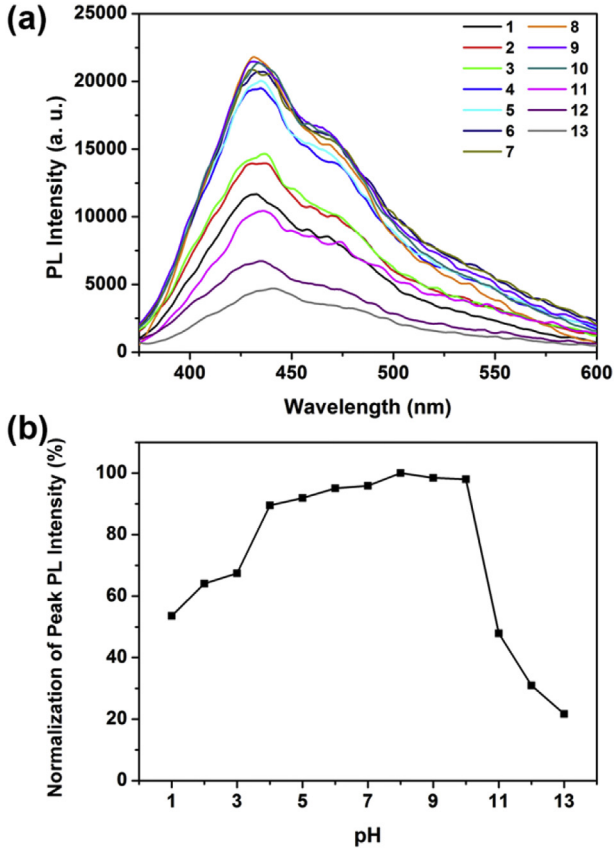

Figure 5. a) PL spectra of 0.05 mg mL^{-1} aGQDs solution at different pH (excitation wavelength = 323 nm), b) the relation plots between PL intensity and pH values.

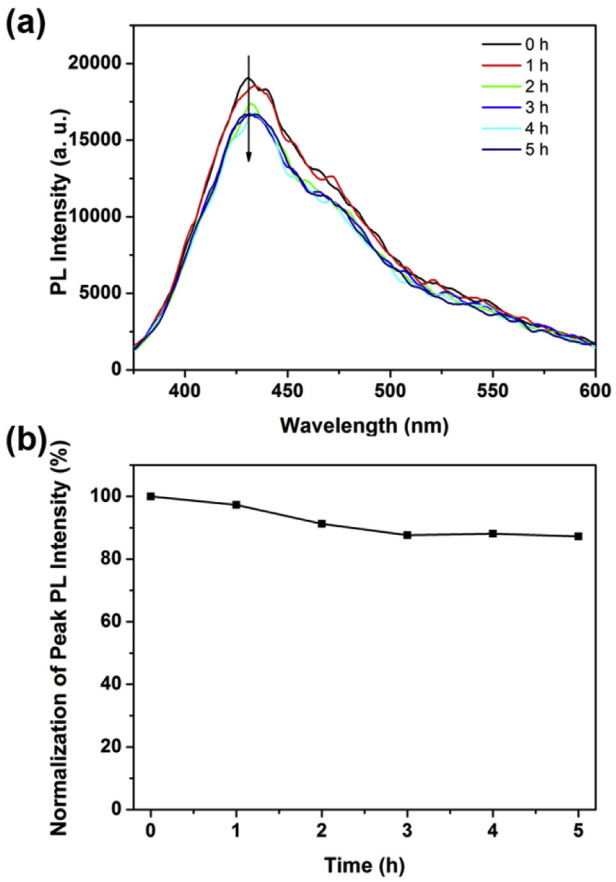

Figure 6. a) Influence of light illumination time on the photoluminescence properties of aGQDs, b) the relation plots between PL intensity and light illumination time.

indicate that the aGQD is a kind of carbonaceous materials with many structural defects together with a large quantity of oxygen-containing functional groups, agreeing well with the images of the HRTEM image.

3.3. Fluorescence properties

The photoluminescence (PL) properties of aGQDs were firstly investigated to evaluate their potential as chemosensor to detect uranyl ions. The PL spectra of different excitation wavelengths are shown in Figure 4. As can be seen, when the excitation wavelength changed from 290 nm to 440 nm, the PL peaks show relevant shifts from 425 nm to 540 nm. Meanwhile, the

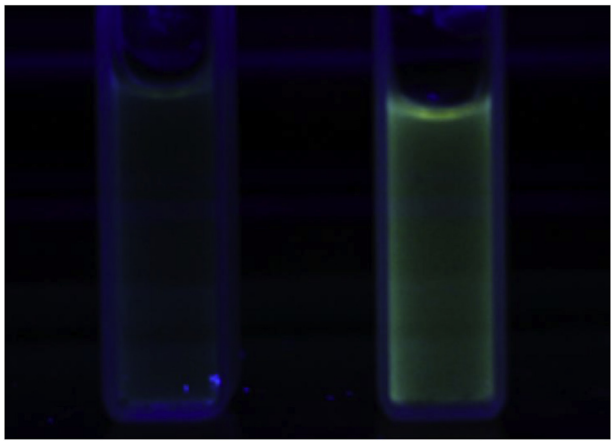

Figure 7. Photographs of uranyl ions' quenching effect on the aGQDs. (The wavelength of UV light is 312 nm)

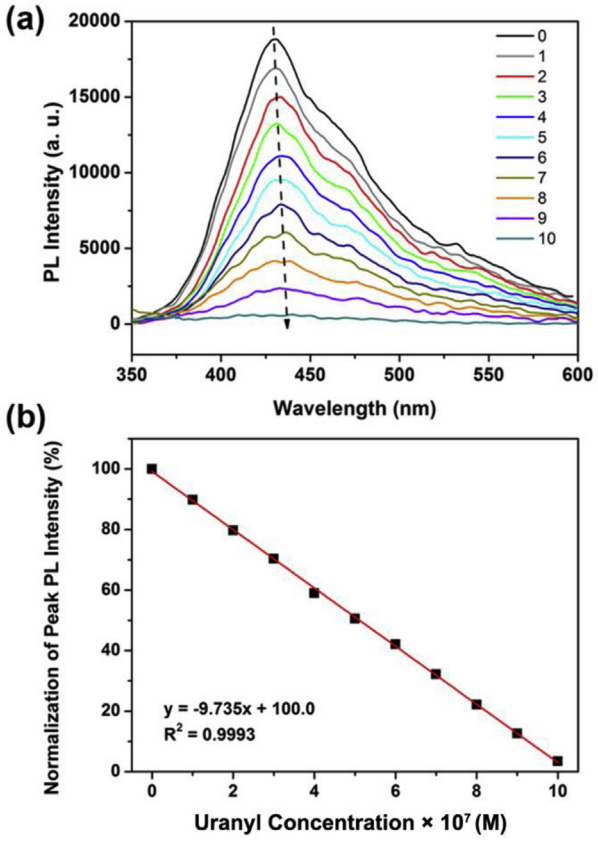

Figure 8. a) Fluorescence quenching effect of uranyl ions on aGQDs solution (c [aGQDs] = 0.05 mg mL^{-1}, pH = 5; 0 was the original FL intensity of aGQDs without any uranyl ions, and 20 μL 10^{-5} M uranyl solution was added into 2 mL aGQDs solution successively from 1 to 10); b) the calibration curve for uranyl ions determination.

intensities of the PL peaks change: firstly, the intensity shows a significant increase after 290 nm; then, when the excitation wavelength reaches 323 nm, the PL peak intensity comes to the top value of all, and the PL peak locates at the wavelength of 427 nm; at last, after 323 nm, the sharp decrease of PL peak intensity also occurs. Therefore, to observe the fluorescence quench of aGQDs brought by uranyl ions, all the experiments mentioned below were conducted at the excitation wavelength of 323 nm.

To further determine the optimized conditions of applying aGQDs as chemosensor material, the influences of pH and natural light illumination time were studied. In a wide pH range from 4 to 10, the PL intensities remain stable; when the pH is <4 or >10, the PL intensities decrease obviously (Figure 5a, b). In other words, the aGQDs could be applied as the chemosensor material within the familiar pH of natural water body. Moreover, the natural light shows no strong quenching effect on aGQDs (Figure 6): at the first 2 h, the PL intensity shows a little decease about 10 %, then the PL intensity remains stable at 90 % of the initial intensity.

3.4. Detection of uranyl ions

As shown in Figure 7, by adding uranyl parent solution into the aGQDs solution to optimize the uranyl concentration around 10^{-6} M, a significant fluorescence quenching effect is observed. The bright yellow-green luminescence almost disappeared. The mechanism of the quenching caused by uranyl ions is mainly due to the coordination between uranyl ions and the carboxyl groups on the aGQDs, which would lead the aggregation of aGQDs, and quench the fluorescence of aGQDs successively. Furthermore, the quantitive relationship between fluorescence quenching effect and uranyl ion concentration were studied by fluorescence spectra (Figure 8). With the increasing concentration of

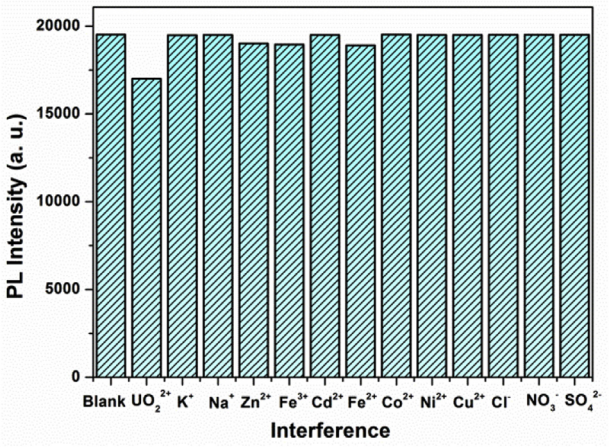

Figure 9. Selectivity of aGQDs as chemosensors. (c[uranyl] = 10^{-7} M, c[other ions] = 10^{-5} M).

uranyl ions, the fluorescence intensity of aGQDs decreased (Figure 8a). A good linear relationship between the concentration of U(VI) and the fluorescence intensity was observed in the range of 10^{-7} to 10^{-6} M with the R^2 of 0.9993 (Figure 8b).

To evaluate the selectivity of aGQDs for uranyl ions, the fluorescence quenching effects of a series of usual ions on aGQDs are compared. The ions, including K^+, Na^+, Zn^{2+}, Fe^{2+}, Cd^{2+}, Fe^{3+}, Co^{2+}, Ni^{2+}, Cu^{2+}, Cl^-, NO_3^-, SO_4^{2-} were taken into consideration. To demonstrate the selectivity, the concentration of uranyl ion was chosen 10^{-7} M, while other ions was chosen 10^{-5} M, 100 times of that of uranyl ion. As shown in Figure 9, uranyl ions cause the most significant fluorescence quenching compared to other metal ions. This may be attributed to the strong coordination interaction between uranyl ions and the oxygen-containing groups of aGQDs. Besides, the slight fluorescence quenching for other metal ions may be a result of the nonspecific interactions between the carboxylic groups and the metal ions. The result showed that the aGQDs have a desirable selectivity for uranyl over a series of ions, which suggested that the aGQDs could be a potential choice as a novel chemosensor for uranyl fluorescence detection with good sensitivity and selectivity.

4. Conclusions

In summary, we have developed a novel synthesis method to prepare graphene quantum dots named as aGQDs via thermal treatment of crude GO in a dry and alkaline condition to cut the crude GO sheets into small graphene quantum dots. The as-prepared aGQDs are rich in oxygen-containing groups which makes them soluble in aqueous condition. The aGQDS aqueous solution shows a bright yellow-green fluorescence under the UV illumination. And the uranyl ions show a strong fluorescence quenching effect on the aGQD aqueous solution even at an ultra-low concentration (~10^{-7} M), which makes the aGQDs a potentially suitable chemosensor for uranyl trace detection. Moreover, the degree of quenching exhibits a fine linear relationship with the concentration of the uranyl ions in the range from 10^{-7} M to 10^{-6} M. Meanwhile, other ordinary ions in water body do not possess the quenching effect or possess much weaker quenching effect on the aGQDs' fluorescence. To sum up, the aGQD is a kind of potential chemosensor for uranyl trace detection with good sensitivity and selectivity.

Declarations

Author contribution statement

Mingfu Chu, Yingru Li and Bianyuan Xia: Conceived and designed the experiments.

Shanli Yang and Yingru Li: Performed the experiments.

Shanli Yang, Yingru Li and Shaofei Wang: Analyzed and interpreted the data.

Shaofei Wang and Jingsong Xu: Contributed analysis tools or data.

Lang Shao, Hao Tang, Yiming Ren and Tao Gai: Contributed reagents, materials, analysis tools or data.

Shanli Yang and Yingru Li: Wrote the paper.

Funding statement

Yingru Li and Shanli Yang were supported by the Initiative Scientific Research Program of Materials Institute (TP02201704, TP02201503). Shanli Yang was supported by the Sichuan Science and Technology Development Foundation for Young Scientists (No. 2017JQ0050). Yiming Ren was supported by the Science Challenge Project (SCP, No. TZ20160040303).

Competing interest statement

The authors declare no conflict of interest.

Additional information

No additional information is available for this paper.

References

[1] Y. Ren, R. Yang, L. Shao, H. Tang, S. Wang, J. Zhao, J. Zhong, C. Kong, The removal of aqueous uranium by SBA-15 modified with phosphoramide: a combined experimental and DFT study, RSC Adv. 6 (2016) 68695–68704.

[2] Y. Ren, H. Tang, L. Shao, J. Zhong, M. Chu, R. Yang, C. Kong, Theoretical study on complexation of U (VI) with ODA, IDA and TDA based on density functional theory, RSC Adv. 6 (2016) 46467–46474.

[3] Y. Sun, J. Li, X. Wang, The retention of uranium and europium onto sepiolite investigated by macroscopic, spectroscopic and modeling techniques, Geochem. Cosmochim. Acta 140 (2014) 621–643.

[4] R.H. Lin, L.J. Wu, C.H. Lee, S.Y. Lin-Shiau, Cytogenetic toxicity of uranyl nitrate in Chinese hamster ovary cells, Mutat. Res. Genet. Toxicol. Test. 319 (1993) 197–226.

[5] A. Hosseini, J.E. Brown, J.P. Gwynn, M. Dowdall, Review of research on impacts to biota of discharges of naturally occurring radionuclides in produced water to the marine environment, Sci. Total Environ. 438 (2012) 325–333.

[6] M. Xu, G. Wei, N. Liu, L. Zhou, C. Fu, M. Chubik, A. Gromova, W. Han, Novel fungus–titanate bio-nanocomposites as high-performance adsorbents for the efficient removal of radioactive ions from wastewater, Nanoscale 6 (2014) 722–725.

[7] M. Altmaier, X. Gaona, T. Fanghänel, Recent advances in aqueous actinide chemistry and thermodynamics, Chem. Rev. 113 (2013) 901–943.

[8] D.P.S. Rathore, Advances in technologies for the measurement of uranium in diverse matrices, Talanta 77 (2008) 9–20.

[9] C.T. Yang, J. Han, M. Gu, J. Liu, Y. Li, Z. Huang, H.Z. Yu, S. Hu, X. Wang, Fluorescent recognition of uranyl ions by a phosphorylated cyclic peptide, Chem. Commun. 51 (2015) 11769–11772.

[10] S.A. Abbasi, Atomic absorption spectrometric and spectrophotometric trace analysis of uranium in environmental samples with N-p-MEthoxyphenyl-2-Furylacrylohydroxamic acid and 4-(2-pyridylazo) resorcinol, Int. J. Environ. Anal. Chem. 36 (1989) 163–172.

[11] A. Lorber, Z. Karpas, L. Halicz, Flow injection method for determination of uranium in urine and serum by inductively coupled plasma mass spectrometry, Anal. Chim. Acta 334 (1996) 295–301.

[12] S. Dhara, N.L. Misra, S.K. Aggarwal, Determination of sulphur in uranium matrix by total reflection X-ray fluorescence spectrometry, Spectrochim. Acta, Part B 63 (2008) 1395–1398.

[13] V. Angeli, S. Biagi, S. Ghimenti, M. Onor, A. D'Ulivo, E. Bramanti, Flow injection-chemical vapor generation atomic fluorescence spectrometry hyphenated system for organic mercury determination: a step forward, Spectrochim. Acta, Part B 66 (2011) 799–804.

[14] R. Brina, A.G. Miller, Direct detection of trace levels of uranium by laser-induced kinetic phosphorimetry, Anal. Chem. 64 (1992) 1413–1418.

[15] C. Ruan, W. Luo, W. Wang, B. Gu, Surface-enhanced Raman spectroscopy for uranium detection and analysis in environmental samples, Anal. Chim. Acta 605 (2007) 80–86.

[16] O. Güney, E. Atçakan, Synthesis and characterization of quinoline-derivated fluorescent sol–gel-imprinted polymer as a chemosensor for sensing of uranyl ion, J. Sol. Gel Sci. Technol. 81 (2017) 534–543.

[17] R.K. Dutta, A. Kumar, Highly sensitive and selective method for detecting ultratrace levels of aqueous uranyl ions by strongly photoluminescent-responsive amine-modified cadmium sulfide quantum dots, Anal. Chem. 88 (2016) 9071–9078.

[18] Z. Wang, Y. Lu, H. Yuan, Z. Ren, C. Xu, J. Chen, Microplasma-assisted rapid synthesis of luminescent nitrogen-doped carbon dots and their application in pH sensing and uranium detection, Nanoscale 7 (2015) 20743–20748.
[19] L.A. Ponomarenko, F. Schedin, M.I. Katsnelson, R. Yang, E.W. Hill, K.S. Novoselov, A.K. Geim, Chaotic Dirac billiard in graphene quantum dots, Science 320 (2008) 356.
[20] S. Zhu, S. Tang, J. Zhang, B. Yang, Control the size and surface chemistry of graphene for the rising fluorescent materials, Chem. Commun. 48 (2012) 4527.
[21] S.Y. Lim, W. Shen, Z. Gao, Carbon quantum dots and their applications, Chem. Soc. Rev. 44 (2015) 362–381.
[22] S. Hu, A. Trinchi, P. Atkin, I. Cole, Tunable photoluminescence across the entire visible spectrum from carbon dots excited by white light, Angew. Chem. Int. Ed. 54 (2015) 2970–2974.
[23] S. Sahu, B. Behera, T.K. Maiti, S. Mohapatra, Simple one-step synthesis of highly luminescent carbon dots from orange juice: application as excellent bio-imaging agents, Chem. Commun. 48 (2012) 8835.
[24] S. Zhuo, M. Shao, S.T. Lee, Upconversion and downconversion fluorescent graphene quantum dots: ultrasonic preparation and photocatalysis, ACS Nano 6 (2012) 1059.
[25] Y. Li, Y. Zhao, H. Cheng, Y. Hu, G. Shi, L. Dai, L. Qu, Nitrogen-doped graphene quantum dots with oxygen-rich functional groups, J. Am. Chem. Soc. 134 (2012) 15.
[26] X. Yan, Q. Li, L.S. Li, Formation and stabilization of palladium nanoparticles on colloidal graphene quantum dots, J. Am. Chem. Soc. 134 (2012) 16095.
[27] L.L. Li, J. Ji, R. Fei, C.Z. Wang, Q. Lu, J.R. Zhang, L.P. Jiang, J.J. Zhu, A facile microwave avenue to electrochemiluminescent two-color graphene quantum dots, Adv. Funct. Mater. 22 (2012) 2971.
[28] Y. Li, Y. Hu, Y. Zhao, G. Shi, L. Deng, Y. Hou, L. Qu, An electrochemical avenue to green-luminescent graphene quantum dots as potential electron-acceptors for photovoltaics, Adv. Mater. 23 (2011) 776.
[29] V. Gupta, N. Chaudhary, R. Srivastava, G.D. Sharma, R. Bhardwaj, S. Chand, Luminscent graphene quantum dots for organic photovoltaic devices, J. Am. Chem. Soc. 133 (2011) 9960.
[30] X. Yan, X. Cui, B. Li, L.S. Li, Large, solution-processable graphene quantum dots as light absorbers for photovoltaics, Nano Lett. 10 (2010) 1869.
[31] M. Xu, S. Xu, Z. Yang, M. Shu, G. He, D. Huang, L. Zhang, L. Li, D. Cui, Y. Zhang, Hydrophilic and blue fluorescent N-doped carbon dots from tartaric acid and various alkylol amines under microwave irradiation, Nanoscale 7 (2015) 15915–15923.
[32] X. Liu, N. Zhang, T. Bing, D. Shangguan, Carbon dots based dual-emission silica nanoparticles as a ratiometric nanosensor for Cu^{2+}, Anal. Chem. 86 (2014) 2289–2296.
[33] A. Gupta, A. Chaudhary, P. Mehta, C. Dwivedi, S. Khan, N.C. Verma, C.K. Nand45i, Nitrogen-doped, thiol-functionalized carbon dots for ultrasensitive Hg (II) detection, Chem. Commun. 51 (2015) 10750–10753.
[34] I. Costas-Mora, V. Romero, I. Lavilla, C. Bendicho, In situ building of a nanoprobe based on fluorescent carbon dots for methylmercury detection, Anal. Chem. 86 (2014) 4536–4543.
[35] Z. Zhang, D. Zhang, C. Shi, W. Liu, L. Chen, M. Yu, D. Juan, J. Li, S. Wang, 3,4-Hydroxypyridinone-modified carbon quantum dot as a highly sensitive and selective fluorescent probe for rapid detection of uranyl ions, Environ. Sci. Nano 6 (2019) 1457–1465.
[36] S. Huang, W. Li, P. Han, X. Zhou, J. Cheng, H. Wen, W. Xue, Carbon quantum dots: synthesis, properties, and sensing applications as a potential clinical analytical method, Anal. Methods 11 (2019) 2240–2258.
[37] Y. Sun, S. Wang, C. Li, P. Luo, L. Tao, Y. Wei, G. Shi, Large scale preparation of graphene quantum dots from graphite with tunable fluorescence properties, Phys. Chem. Chem. Phys. 15 (2013) 9907–9913.
[38] C. Hu, C. Yu, M. Li, X. Wang, Q. Dong, G. Wang, J. Qiu, Nitrogen-doped carbon dots decorated on graphene: a novel all-carbon hybrid electrocatalyst for enhanced oxygen reduction reaction, Chem. Commun. 51 (2015) 3419–3422, 2015.
[39] S. Zhu, Q. Meng, L. Wang, J. Zhang, Y. Song, H. Jin, K. Zhang, H. Sun, H. Wang, B. Yang, Highly photoluminescent carbon dots for multicolor patterning, sensors, and bioimaging, Angew. Chem. Int. Ed. 52 (2013) 3953–3957.
[40] P. Rumbach, M. Witzke, R.M. Sankaran, D.B. Go, Decoupling interfacial reactions between plasmas and liquids: charge transfer vs plasma neutral reactions, J. Am. Chem. Soc. 135 (2013) 16264–16267.
[41] C. Li, C. Yu, C. Wang, S. Chen, Decoupling interfacial reactions between plasmas and liquids: charge transfer vs plasma neutral reactions, J. Mater. Sci. 48 (2013) 6307–6311.
[42] Q. Lu, C. Wu, D. Liu, H. Wang, W. Su, H. Li, Y. Zhang, S. Yao, A facile and simple method for synthesis of graphene oxide quantum dots from black carbon, Green Chem. 19 (2017) 900–904.
[43] J. Chen, Y. Li, L. Huang, C. Li, G. Shi, High-yield preparation of graphene oxide from small graphite flakes via an improved Hummers method with a simple purification process, Carbon 81 (2015) 826–834.
[44] Y. Li, J. Chen, L. Huang, C. Li, G. Shi, "Pottery" of porous graphene materials, Adv. Electron. Mater. 1 (2015) 1500004.
[45] Y. Li, J. Zhao, C. Tang, Y. He, Y. Wang, J. Chen, J. Mao, Q. Zhou, B. Wang, F. Wei, J. Luo, G. Shi, Highly exfoliated reduced graphite oxide powders as efficient lubricant oil additives, Adv. Mater. Interfaces 3 (2016) 1600700.
[46] A.M. Dimiev, L.B. Alemany, J.M. Tour, Graphene oxide. Origin of acidity, its instability in water, and a new dynamic structural model, ACS Nano 7 (2013) 576–588.
[47] Y. Li, Y. Hu, Y. Zhao, G. Shi, L. Deng, Y. Hou, L. Qu, An electrochemical avenue to green-luminescent graphene quantum dots as potential electron-acceptors for photovoltaics, Adv. Mater. 23 (2011) 776.